LAWRENCE
LIVERMORE
NATIONAL
LABORATORY

UCRL-JRNL-217959

Deducing the 237U(n,f) cross-section using the Surrogate Ratio Method

J. T. Burke, L. A. Bernstein, J. Escher, L. Ahle, J. A. Church, F. S. Dietrich, K. J. Moody, E. B. Norman, L. Phair, P. Fallon, R. M. Clark, M. A. Deleplanque, M. Descovich, M. Cromaz, I. Y. Lee, A. O. Macchiavelli, M. A. McMahan, L. G. Moretto, E. Rodriguez-Vieitez, F. S. Stephens, H. Ai, C. Beausang, B. Cridder

January 5, 2006

Physical Review C

Deducing the ^{237}U(n,f) cross-section using the Surrogate Ratio Method

J.T. Burke,* L.A. Bernstein, J. Escher, L. Ahle, J.A. Church, F.S. Dietrich, K.J. Moody, and E.B. Norman
Lawrence Livermore National Laboratory, Livermore, California, 94551

L. Phair, P. Fallon, R.M. Clark, M.A. Deleplanque, M. Descovich, M. Cromaz, I.Y. Lee, A.O. Macchiavelli, M.A. McMahan, L.G. Moretto, E. Rodriguez–Vieitez, and F.S. Stephens
Lawrence Berkeley National Laboratory, Berkeley, California, 94720

H. Ai
Yale University, New Haven, Connecticut, 06520

C. Beausang and B. Cridder
University of Richmond, Richmond, Virginia, 23173
(Dated: January 25, 2006)

We have deduced the cross section for ^{237}U(n,f) over an equivalent neutron energy range from 0 to 20 MeV using the Surrogate Ratio method. A 55 MeV ^{4}He beam from the 88 Inch Cyclotron at Lawrence Berkeley National Laboratory was used to induce fission in the following reactions: $^{238}U(\alpha,\alpha' f)$ and $^{236}U(\alpha,\alpha' f)$. The ^{238}U reaction was a surrogate for $^{237}U(n,f)$ and the ^{236}U reaction was used as a surrogate for $^{235}U(n,f)$. Scattered alpha particles were detected in a fully depleted segmented silicon telescope array (STARS) over an angle range of 35^o to 60^o with respect to the beam axis. The fission fragments were detected in a third independent silicon detector located at backward angles between 106^o to 131^o.

PACS numbers: 24.50.+g, 24.75.+i, 25.55.-e, 25.55.Ci, 25.85.Ge, 29.40.Wk
Keywords: surrogate reaction, direct reaction, ratio method, fission

I. INTRODUCTION

Neutron-induced fission cross sections are of interest for a variety of applied and basic science reasons. To further our understanding of fission we have employed the "Surrogate Ratio method" described by Plettner et al. [1, 2] to determine the ^{237}U(n,f) cross section via comparison with the well-measured ^{235}U(n,f) cross section. This technique removes and/or reduces a large number of systematic and theoretical uncertainties related to the direct Surrogate Method [3, 4]. In this report, we review the Surrogate Ratio method as it pertains to fission, describe the experiment, and present the resulting ^{237}U(n,f) deduced cross section.

II. THE SURROGATE RATIO METHOD

The "Surrogate Ratio method" or, simply, the "Ratio method" is an indirect technique that allows the determination of cross sections for compound-nucleus reactions involving difficult-to-produce targets. The method is a variant of the so-called "Surrogate nuclear reaction approach" in that it uses a light-ion induced reaction to determine the decay probability of the same compound nucleus (CN) that occurs in the desired difficult-to-measure reaction. However, the Ratio method requires that the decay probabilities of two similar CN are measured relative to one another. The second CN has to occur in a reaction that is similar to the difficult-to-measure desired reaction and for which the cross section is known. In this report we use the known ^{235}U(n,f) cross section to obtain the cross section for ^{237}U(n,f) for neutron energies up to 20 MeV. The following reviews the Surrogate nuclear reaction idea, explains the motivation for considering simplifications of the approach, and outlines the Ratio method.

The Surrogate nuclear reaction technique is an indirect method to determine the cross section for a particular type of "desired" reaction, $a + A \rightarrow B^* \rightarrow c + C$, that proceeds through a CN state B^*, which is a highly excited state in statistical equilibrium [5–14]. The formation and decay of a CN with a given angular momentum and parity are independent of each other. In such situations, the cross section for the desired reaction can be (somewhat schematically) expressed as

$$\sigma_{\alpha\chi}(E_a) \;=\; \sum_{J,\pi} \sigma_{\alpha}^{CN}(E_{ex},J,\pi)\;\; G_{\chi}^{CN}(E_{ex},J,\pi)\;. \quad (1)$$

Here α denotes the entrance channel $a + A$ and χ represents the relevant exit channel $c + C$. E_a is the kinetic energy of the projectile a and E_{ex} is the excitation energy of the compound nucleus B^*; they are related via the separation energy S_a of the projectile in the nucleus B: $E_{ex} = S_a + E_a$. In this present work, we are interested in the reactions $n+^{235}$U $\rightarrow$ ^{236}U* $\rightarrow$ *fission* and

*Electronic address: burke26@llnl.gov

$n+^{237}\mathrm{U} \rightarrow {}^{238}\mathrm{U}^* \rightarrow$ *fission*. In many cases the formation cross section $\sigma_\alpha^{CN} = \sigma(a + A \rightarrow B^*)$ can be calculated adequately by using optical potentials, while the theoretical decay probabilities G_χ^{CN} for the different channels χ are often quite uncertain. The objective of the Surrogate method is to determine or constrain these decay probabilities experimentally.

In a Surrogate experiment, the compound nucleus B^* is produced via an alternative ("Surrogate"), direct reaction $d+D \rightarrow b+B^*$ and the decay of B^* is observed in coincidence with the outgoing particle b. In the experiment, the relevant compound nuclei $^{236}\mathrm{U}^*$ and $^{238}\mathrm{U}^*$ were produced via inelastic alpha scattering, $^{236,238}\mathrm{U}(\alpha,\alpha')$. Fission fragments were detected in coincidence with scattered alpha particles. The probability for forming B^* in the Surrogate reaction (with specific values for the excitation energy E_{ex}, angular momentum J, and parity π) is $F_\delta^{CN}(E_{ex}, J, \pi)$, where δ refers to the entrance channel $d+D$. The quantity

$$P_{\delta\chi}(E_{ex}) = \sum_{J,\pi} F_\delta^{CN}(E_{ex}, J, \pi)\ G_\chi^{CN}(E_{ex}, J, \pi)\ , \quad (2)$$

which gives the probability that the compound nucleus B^* was formed with energy E_{ex} and decayed into channel χ, can in principle be obtained experimentally.

The direct-reaction probabilities $F_\delta^{CN}(E_{ex}, J, \pi)$ have to be determined theoretically, so that the branching ratios $G_\chi^{CN}(E_{ex}, J, \pi)$ can be extracted from the measurements. In practice, the decay of the compound nucleus is modeled using statistical reaction theory and the $G_\chi^{CN}(E_{ex}, J, \pi)$ are obtained by adjusting parameters in the calculations to reproduce the measured decay probabilities $P_{\delta\chi}(E_{ex})$. Subsequently, the branching ratios obtained in this manner are inserted in equation 1 to yield the desired reaction cross section.

The experimental determination of the decay probability $P_{\delta\chi}(E_{ex}) = N_{\delta\chi}/N_\delta$ requires that both the number of b-χ coincidences ($N_{\delta\chi}$) and the number of reaction events (N_δ) (the total number of inelastically scattered alpha particles in the present case) are accurately determined. If target contaminants are present, it becomes very difficult, if not impossible to determine a reliable value for N_δ.

The "Surrogate Ratio method" eliminates the need to accurately measure N_δ, the total number of reaction events, which has been the source of the largest uncertainty in Surrogate experiments performed recently [1, 3]. Under the proper circumstances it also reduces or removes dependence on the angular distribution of fission fragments, which is not well characterized in the present experiments. The goal of the Ratio method is to experimentally determine the ratio

$$R(E) \ = \ \frac{\sigma_{\alpha_1\chi_1}(E)}{\sigma_{\alpha_2\chi_2}(E)} \quad (3)$$

of the cross sections of two compound-nucleus reactions, $a_1 + A_1 \rightarrow B_1^* \rightarrow c_1 + C_1$ and $a_2 + A_2 \rightarrow B_2^* \rightarrow c_2 + C_2$, for the same excitation energy, $E \equiv E_{ex_1} = E_{ex_2}$ of both compound nuclei. An independent determination of one of the above cross sections then allows one to infer the other by using the ratio $R(E)$.

Under certain conditions [15, 16] the branching ratios $G_\chi^{CN}(E_{ex}, J, \pi)$ become independent of J and π, i.e. the Weisskopf-Ewing limit of the statistical Hauser-Feshbach theory applies. The form of the cross section (for the desired reaction) simplifies to $\sigma_{\alpha\chi}^{WE}(E_{ex}) = \sigma_\alpha^{CN}(E_{ex})\ \mathcal{G}_\chi^{CN}(E_{ex})$ where $\sigma_\alpha^{CN}(E_{ex}) = \sum_{J\Pi} \sigma_\alpha^{CN}(E_{ex}, J, \pi)$ is the reaction cross section describing the formation of the compound nucleus at energy E_{ex} and $\mathcal{G}_\chi^{CN}(E_{ex})$ denotes the $J\pi$-independent branching ratio for the exit channel χ. In the Weisskopf-Ewing limit, the ratio $R(E_{ex})$ can be written as:

$$R(E_{ex}) \ = \ \frac{\sigma_{\alpha_1}^{CN}(E_{ex})\ \mathcal{G}_{\chi_1}^{CN}(E_{ex})}{\sigma_{\alpha_2}^{CN}(E_{ex})\ \mathcal{G}_{\chi_2}^{CN}(E_{ex})}\ , \quad (4)$$

with branching ratios $\mathcal{G}_\chi^{CN}$ that are independent of the $J\pi$ population of the compound nuclei under consideration. For most cases of interest the compound-nucleus formation cross sections $\sigma_{\alpha_1}^{CN}$ and $\sigma_{\alpha_2}^{CN}$ can be calculated using an optical model. To determine $\mathcal{G}_{\chi_1}^{CN}/\mathcal{G}_{\chi_2}^{CN}$, two experiments are carried out. Both use the same direct-reaction mechanism $D(d,b)B^*$, but different targets D_1 and D_2 to create the relevant compound nuclei B_1^* and B_2^* respectively. For each experiment, the number of coincidence events, $N_{\delta_1\chi_1}^{(1)}$ and $N_{\delta_2\chi_2}^{(2)}$, are measured.

In the present case, $^{236}\mathrm{U}(\alpha,\alpha')^{236}\mathrm{U}^*$ and $^{238}\mathrm{U}(\alpha,\alpha')^{238}\mathrm{U}^*$ experiments were carried out and α-*fission* coincidences were measured. The same experimental setup was employed for both cases. The ratio of the branching ratios into the desired channel for the compound nuclei created in the two reactions is given by

$$\frac{\mathcal{G}_{\chi_1}^{CN}(E_{ex})}{\mathcal{G}_{\chi_2}^{CN}(E_{ex})} \ = \ \frac{N_{\delta_1\chi_1}^{(1)}(E_{ex})}{N_{\delta_2\chi_2}^{(2)}(E_{ex})} \times \frac{N_{\delta_2}^{(2)}(E_{ex})}{N_{\delta_1}^{(1)}(E_{ex})}\ . \quad (5)$$

If both experiments give the same number of reaction events, $N_{\delta_1}^{(1)} \approx N_{\delta_2}^{(2)}$, the ratio of the decay probabilities simply equals the ratio of the coincidence events and the quantity $R(E_{ex})$ becomes:

$$R(E_{ex}) \ = \ \frac{\sigma_{\alpha_1}^{CN}(E_{ex})\ N_{\delta_1\chi_1}^{(1)}(E_{ex})}{\sigma_{\alpha_2}^{CN}(E_{ex})\ N_{\delta_2\chi_2}^{(2)}(E_{ex})}\ . \quad (6)$$

In practice it is unlikely that both experiments yield the same number of reaction events and it becomes necessary to apply a correction to account for the difference in target thickness, integrated beam on target, and live time of the data acquisition for the two experiments.

III. EXPERIMENTAL APPARATUS

The present experiment was performed at the 88 Inch Cyclotron at Lawrence Berkeley National Labo-

ratory using the Silicon Telescope Array for Reactions Studies (STARS) developed by Lawrence Livermore National Laboratory. Inelastically scattered alpha particles from the $^{238}U(\alpha,\alpha' f)$ and $^{236}U(\alpha,\alpha' f)$ reactions were detected using the STARS scattering chamber shown schematically in figure 1. The silicon telescope produces differential energy loss in the thin (ΔE) and thick (E) detectors which enables particle identification. The ΔE and E detectors were both Micron "S2" type with a thickness of 140 μm and 1000 μm respectively. Each S2 detector has 48 rings on one side and 16 sectors on the other. For this experiment both detectors had pairs of adjacent rings and sectors bussed together to form twenty-four 1 mm wide rings and 8 sectors. The targets were located 16 mm upstream from the front face of the ΔE detector. The ΔE and E detectors were spaced 3 mm apart. The beam spot on the target was approximately 3 mm in diameter. This geometry leads to an angular detection range in θ (the angle formed between the beam axis and the scattered alpha particle) from 35^o to 60^o. The trajectory of an alpha particle was determined by which rings in the ΔE and E detector were triggered. The angular resolution limited the precision of the recoil energy correction applied to the scattered α-particle. A 4.44 $\frac{mg}{cm^2}$ aluminum foil was placed between the target and the silicon telescope. The aluminum foil served a dual purpose. The foil ranged out the fission fragments thereby protecting the ΔE detector from damage which would reduce its energy resolution. The foil was also biased to 300 V during the experiment to help reduce the effect of delta electrons produced in the target. Fission fragments were detected in a third 140 μm Micron S2 detector located 10 mm upstream of the target. The adjacent rings and sectors of this detector were also bussed together. The fission detector covered an angle range of 106^o to 131^o with respect to the beam axis of the telescope.

The ΔE, E, and fission detectors were biased with 30 V, 105 V, and 30 V respectively. The signals from the rings and sectors of the ΔE and E detector were conducted through the vacuum chamber wall by four straight-through 34 pin connectors potted into a custom made NEMA-G10 vacuum flange. The signals were pre-amplified by 64 individual 45 mV/MeV CHARGE8V Swan Research pre-amplifiers located on the side of the STARS scattering chamber. The amplified signals were connected to four 16 channel CAEN N568B shapers by 64 individual 10 m long RG-174 cables. The signals from the fission detector were treated identically with the exception that the pre-amplifiers used had a sensitivity of 8 mV/MeV. The fast output of the CAEN N568B shapers were connected to LeCroy 1806 discriminators modified to be leading edge. The discriminator thresholds were set at 60 mV which corresponds to an energy threshold of approximately 800 keV. At least one hit in each ΔE and E detector were required to form the particle trigger. Once a valid trigger occured, the delayed shaped slow output of the shaper channels were digitized by 96 channels of SILENA analog to digital converters (ADCs). The gate

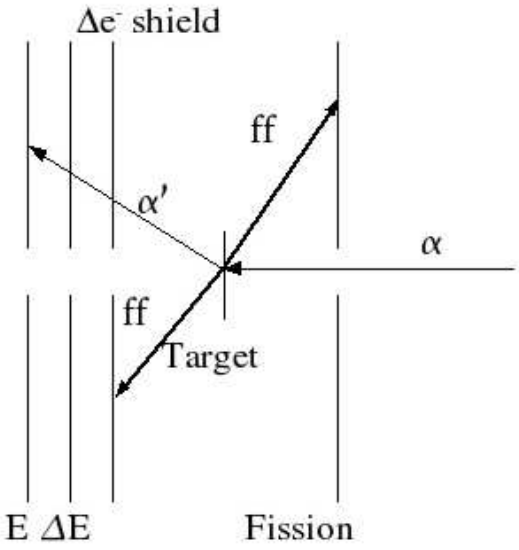

FIG. 1: Schematic view of the STARS detector setup. The silicon telescope is downstream from the target. The fission detector is located 10 mm upstream of the target. The Δe^- shield located in front of the ΔE detector ranged out the fission fragments.

provided to the SILENA ADCs was approximately 7 μs long. Particle-fission timing was obtained using a Time-to-Amplitude module read out using an Ortec AD413 Peak-sensing ADC.

IV. DETECTOR CALIBRATION

The ΔE and E silicon detectors were calibrated using a ^{226}Ra alpha source. A typical calibration spectrum is shown in figure 2. The peaks were fit with a skewed Gaussian in order to account for the effects of incomplete charge collection in the silicon. Typical values for σ were between 31 to 46 keV for the rings on the ΔE detector and 22 to 30 keV for the rings on the E detector. The sectors of both detectors had a factor of approximately 1.4 poorer energy resolution (ΔE/E). In order to obtain the best energy resolution possible the rings were used to reconstruct the energy of the alpha particle events. The 1σ energy resolution of the combined detectors was taken as the sum of the squares of the individual uncertainties and ranged between 38 keV to 55 keV.

V. OBSERVATIONS

Data were taken over a period of five consecutive days at the 88 Inch Cyclotron using a 55 MeV beam of α-particles with an intensity between 2 to 5 pnA. The ΔE-E overlap coincidence time window was adjusted to be ap-

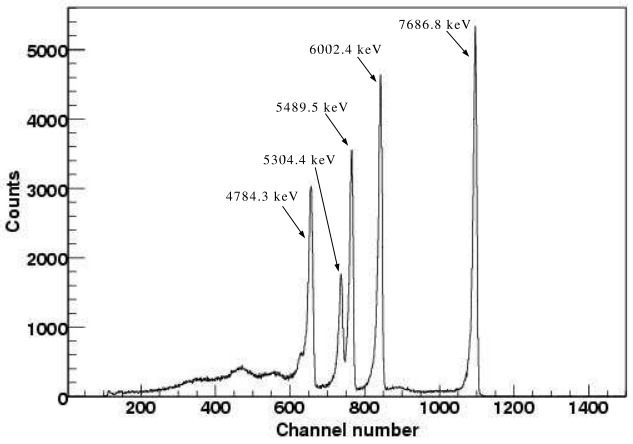

FIG. 2: A typical ^{226}Ra calibration spectrum for an individual ring. The data show the five dominant alpha particles present in the ^{226}Ra decay chain versus channel number in the SILENA ADC.

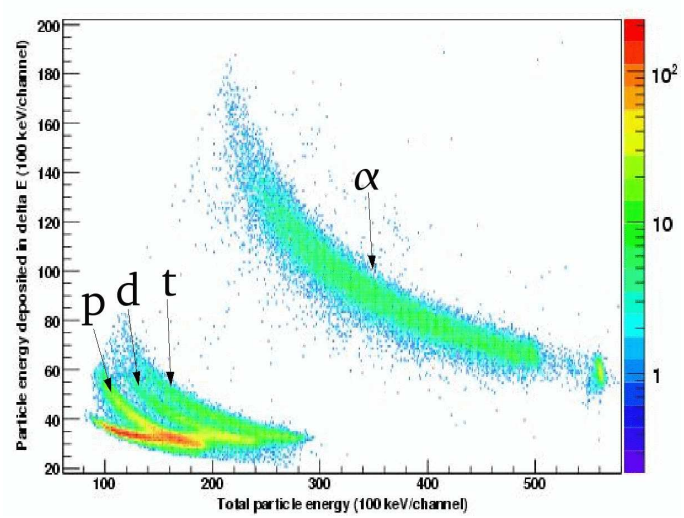

FIG. 3: Delta E versus E plot obtained from nominally 55 MeV alpha particle incident on ^{238}U in coincidence with fission events. Starting in the lower left corner we see protons, deuterons, and tritons. The large band in the middle of the plot represents alpha particles.

proximately 50 ns. The ^{238}U fission data were obtained from a self supporting metallic 3619 ± 72 angstrom (585 ± 23 $\frac{\mu g}{cm^2}$) thick ^{238}U foil. The ^{236}U fission data were obtained using a uranyl nitrate $^{236}UO_2(NO_3)_2$ target consisting of 99.68% ^{236}U and 0.32% ^{234}U electroplated onto a 2.3 $\frac{mg}{cm^2}$ Ta foil. The ^{236}U foil had an areal density of approximately 184 ± 9 $\frac{\mu g}{cm^2}$. The areal density of each target was determined by its area and specific activity. The master trigger rate for coincident events ranged between 4 kHz to 6 kHz during the experiment. The data acquisition system event deadtime was set by the master gate width of 70 μs. At master trigger rates of 4 kHz and 6 kHz the system deadtime was 28 % and 42 % respectively. The fission detector singles rate was considerably higher at 40 kHz. This was due to a large (approximately 1 barn) ^{238}U(α, f) fusion-fission cross section.

The protons, deuterons, tritons, ^{3}He and alpha particles were uniquely identified by plotting the ΔE energy against the total energy (ΔE + E) to create a particle identification (PID) plot as shown in figure 3. The PID plot for each ring was linearized to create an effective thickness versus energy plot. The effective thickness versus energy plot was generated using the following linearization function where R is the range, E_{tot} is the total particle energy, and E is the energy deposited in the E detector.

$$R = 15.0 \times (E_{tot}^{1.75} - E^{1.75}) \quad (7)$$

Figure 4 shows a typical effective thickness energy curve for an individual ring. Alpha particle events were defined as particles that occured within an energy range of 2σ (approximately 400 keV) of the centroid of the alpha particle band. This range energy cutoff ensures that the data from the ^{236}U and ^{238}U are free from (^{4}He,^{3}He) induced fission events. Events in the fission detector

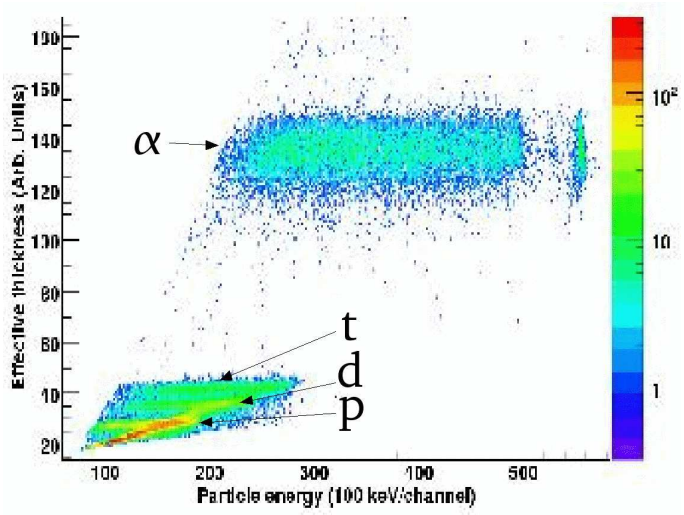

FIG. 4: Effective thickness energy curve. Alpha particles can be seen in the top band. The three bands in the lower left hand corner starting from the bottom are protons, deuterons, and tritons respectively.

greater than 6 MeV (approximately channel 200 in figure 5) were identified as fission events to remove light ions from direct reactions and charged-particle evaporation. The fission fragments lose considerable energy in the target and detector dead layer before they are detected. A typical fission spectrum for an individual ring is shown in figure 5. The uncertainty in determining the cut off point at the minimum of the fission spectrum introduces a systematic uncertainty in the final ^{237}U(n,f) cross section. The sensitivity of the final cross section to the fission cutoff point was determined to be 1.3% and is

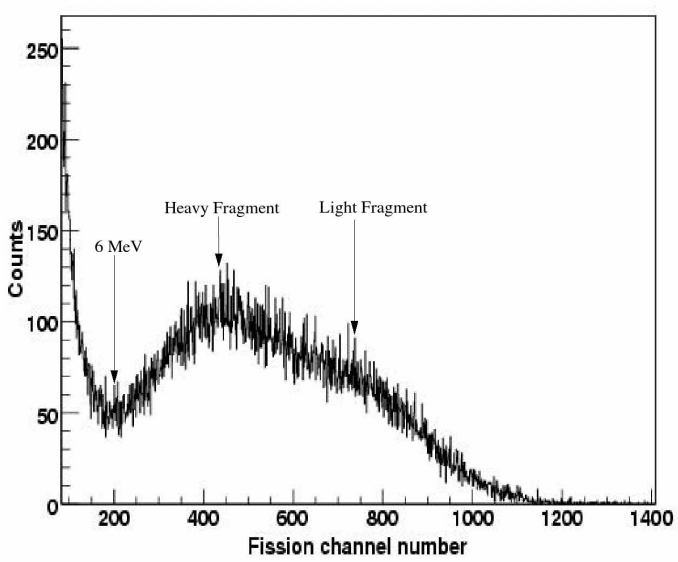

FIG. 5: Typical fission spectrum from a ring in the fission detector. The centroid of the light and heavy fission fragments are indicated with arrows.

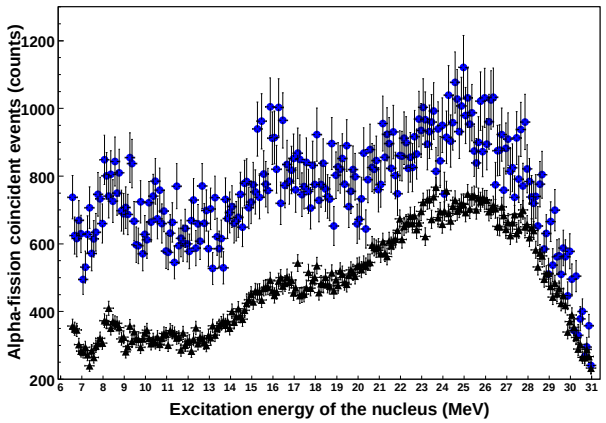

FIG. 6: Number of $(\alpha, \alpha' f)$ events as a function of excitation energy of the respective nucleus. This data is used to calculate relative probability of fission for ^{238}U compared to ^{236}U. The ^{236}U data are represented by circles and the ^{238}U data are shown as triangles.

listed in Table I.

For each ring in the ΔE detector a PID plot and range curve were created. The alpha particles, identified in the effective thickness energy plot, in coincidence with fission events were identified by the sort routine. A histogram of alpha-fission coincidences as a function of alpha particle energy was created for each ring in the ΔE detector. The energy bins for the histogram were chosen to be 100 keV wide. A bin size of 100 keV was chosen due to the statistics per bin and in order to allow for compression at a later time. The alpha particle energy was corrected event by event for recoil effects and for energy losses in the target, aluminum δ-shield, and inert detector layers (Al and Au). The spectra for each ring were then summed together. This process was identical for both $^{238}U(\alpha, \alpha' f)$ and the $^{236}U(\alpha, \alpha' f)$ data. The data were also corrected to take into account the integrated beam current, number of target atoms, and live time of the acquisition system. This normalization factor is

$$Norm = \frac{I_{^{236}U}}{I_{^{238}U}} \times \frac{T_{Live^{236}U}}{T_{Live^{238}U}} \times \frac{N_{Atoms^{236}U}}{N_{Atoms^{238}U}} = 0.1534 \quad (8)$$

where $I_{^{23x}U}$ is the integrated beam current, $T_{Live^{23x}U}$ is the live time fraction, and $N_{Atoms^{23x}U}$ are the number of atoms of the corresponding target. The uncertainties associated with the live time fraction and integrated beam current are less than a percent. The uncertainty in the target thicknesses mentioned above is the dominant uncertainty in the normalization factor and is listed in Table I.

The final alpha fission spectra are given by

$$N(E_{ex})_{^{238}Ufission} = N(E_{ex})_{^{238}U\alpha-f} \quad (9)$$

and

$$N(E_{ex})_{^{236}Ufission} = \frac{N(E_{ex})_{^{236}U\alpha-f}}{Norm} \quad (10)$$

where $N(E_{ex})_{^{23x}Ufission}$ are the corrected fission spectra, $N(E_{ex})_{^{23x}U\alpha-f}$ are the alpha fission coincident spectra described above, and $Norm$ is the normalization factor from equation (8). Figure 6 shows the resulting spectra corrected for the normalization factor. The α-U Coulomb barrier (24 MeV) and the recoil of the target nucleus limit the maximum excitation energy that can be studied to approximately 26 MeV.

VI. SYSTEMATIC UNCERTAINTIES

A detailed analysis of the energy loss and uncertainty in the detector system has been performed. The sources of uncertainty are energy straggle, angular resolution, intrinsic detector energy resolution, and cyclotron beam energy resolution and they are documented in Table II. The energy straggle arises from the interaction of the alpha particles with the various materials in the target and detector system. Alpha particles interact with the target material, δ-shield, aluminum and gold layers on the detector, and the silicon. The energy losses in the inactive layers are substantial (700 keV to 2 MeV) and are corrected on an event by event basis in the data analysis. The energy loss corrections take into account the energy of the incident alpha particle and the angle at which it is incident. Typical values of energy loss are given in Table III. The angular resolution of the detector is dictated by the geometry of the beam spot on the target and the relative distances of the target to the ΔE and E detectors.

TABLE I: Sources of systematic uncertainty for the ^{238}U/^{236}U ratio.

Affected parameter	Source of uncertainty	Relative uncertainty
Normalization Factor	^{238}U Target thickness	5 %
Normalization Factor	^{236}U Target thickness	5 %
Alpha spectra	Fission spectrum cutoff energy	1.3 %
Total systematic uncertainty		7.2 %

TABLE II: Systematic sources of energy uncertainty.

Sources of sytematic energy uncertainty	ΔE (keV)
Energy straggle (δ-shield and target)	38 – 85
Recoil angle	19 – 54
Intrinsic detector energy resolution	38 – 55
Cyclotron beam	60
Total uncertainty	157 - 220

For this experiment, the angular resolution ranged between 0.7^o to 2.2^o. The angular resolution translates into an uncertainty of the recoil angle of the target nucleus. The intrinsic detector resolution was measured using the ^{226}Ra source described in Section IV. The cyclotron beam energy resolution was inferred from the width of the elastic peak in a previous experiment. In that experiment, the beam width was measured by placing a calibrated silicon detector directly in the alpha beam from the 88 Inch Cyclotron [17]. The energy width of the cyclotron beam was then inferred using the following relation

$$\Delta E^2_{total} = \Delta E^2_{cal} + \Delta E^2_{beam} \quad (11)$$

where E_{total} is the total energy uncertainty, E_{cal} is the intrinsic detector resolution, and E_{beam} is the Cyclotron beam energy width. The energy uncertainty changes as a function of outgoing alpha particle angle, therefore the energy straggle and recoil angle uncertainty partially cancel each other. As a final check on the energy uncertainty, the elastic peak was fit with a gaussian and the 1σ uncertainty was found to be 220 keV. Based on this and the above calculations the overall energy uncertainty used in the final cross section was taken to be 220 keV.

The fission fragments have a distribution with respect to the recoiling nucleus that is anisotropic. This anisotropy changes with the excitation energy of the nucleus. Differences in the anisotropy of the fission fragments [18] with respect to the recoiling ^{236}U and ^{238}U nuclei constitute another source of uncertainty due to the finite solid angle coverage of the fission detector. The fission fragment anisotropies for ^{238}U and ^{236}U fission fragments have been examined as shown in figure 7. As a measure of the anisotropy, we consider the ratio of the number of fission events in the angular range of 0^o to 30^o to the number of fission events over the angle range of 45^o to 80^o, as a function of excitation energy. The angle described here is taken with respect to the recoiling uranium nucleus. In the energy range near the fission barrier, from 0 to 4 MeV surrogate neutron energy (6.4 to 10.4 MeV excitation energy), the anisotropy peaked at a factor of 3 and dropped to unity by 4 MeV surrogate neutron energy for both nuclei. The main feature to note is that the ratio of the fission fragment anisotropies of ^{238}U over ^{236}U was found to be consistent with unity in the energy range from 0 to 20 MeV surrogate neutron energy (6 to 26 MeV in excitation energy). The ratio method reduces our sensitivity to the fission fragment anisotropies provided the two nuclei have similar distributions as is the case here.

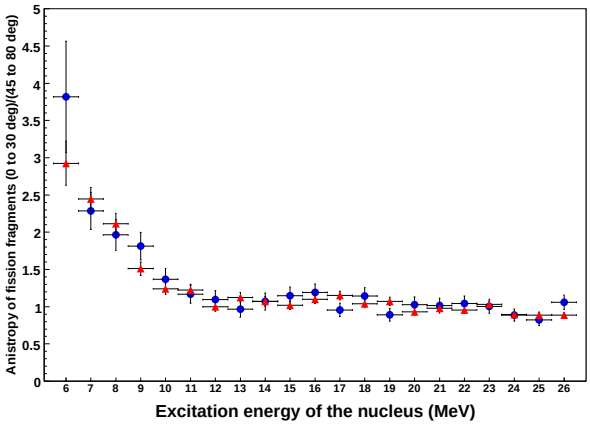

FIG. 7: The in-plane fission fragment anisotropies as a function of excitation energy of the nucleus for ^{238}U (red triangles) and ^{236}U (blue circles). The anisotropy is most pronounced at the fission barrier E$_{ex}$ of approximately 6 MeV and decreases towards unity thereafter. The fission anisotropies are equal within the experimental uncertainties over the excitation energy range of interest.

VII. ^{237}U(n,F) CROSS SECTION RESULTS

The ^{237}U(n,f) cross section was determined from the data using the procedure described in Section II. The normalized ratio $R(\frac{238}{236}) = N(E_{ex},^{238}U_{fission})/N(E_{ex},^{236}U_{fission})$ was determined as a function of excitation energy and is plotted in figure 8. The ^{235}U(n,f) cross section energy scale was converted to excitation energy by adding the ^{236}U neutron separation energy (S$_n$ = 6544.5 keV). The product of the $R(\frac{238}{236})$ ratio and the $^{235}U(E_{ex})$ spectrum yields the $^{237}U(E_{ex},n,f)$ spectrum in excitation energy. The final result is obtained by shifting the $^{237}U(E_{ex},n,f)$

TABLE III: Materials responsible for energy loss.

Detector Element	Material	Areal Density ($\frac{\mu g}{cm^2}$)	E_{loss} (keV)
^{238}U Target	^{238}U	292	18 - 52
^{236}U Target	^{236}U	92	6 - 15
^{181}Ta Backing (^{236}U target only)	^{181}Ta	2300	150 - 418
Delta Shield	Aluminum	4440	508 - 1534
Detector Contacts (sectors)	Gold	1158	73 - 200
Detector Contacts (rings)	Aluminum	27	19 - 33
Total energy loss for ^{238}U target and detector			682 - 1744
Total energy loss for ^{236}U target and detector			838 - 2128

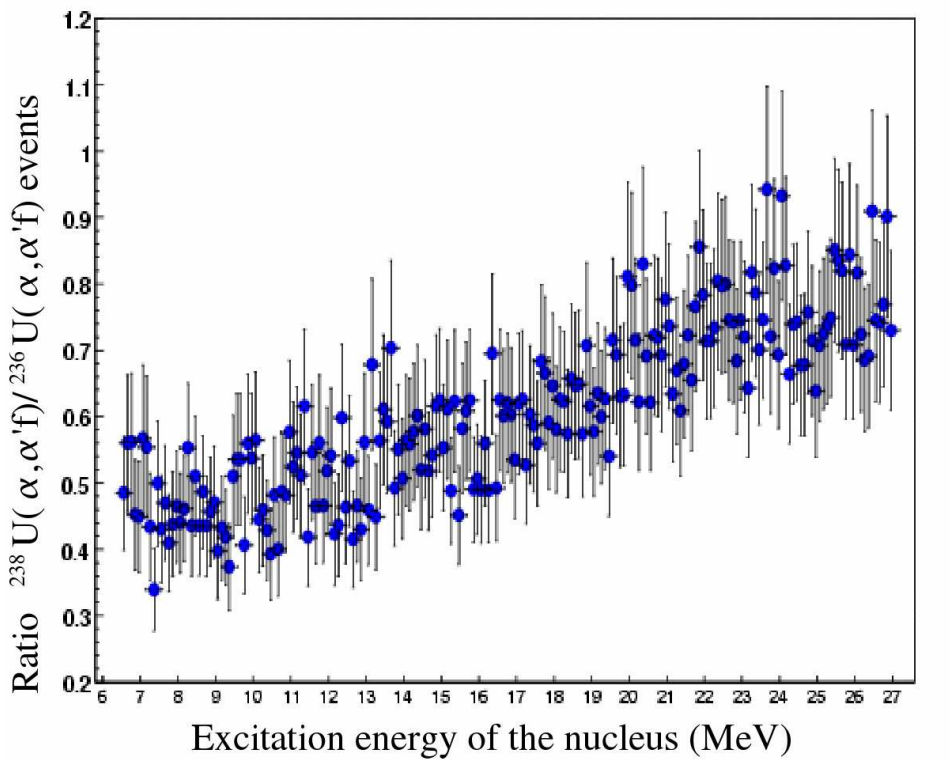

FIG. 8: The ratio of $^{238}U(\alpha,\alpha' f)$ to $^{236}U(\alpha,\alpha' f)$ events as a function of excitation energy of the corresponding nucleus.

energy scale down by subtracting the ^{238}U neutron separation energy (S_n = 6152.0 MeV) to obtain the $^{237}U(n,f)$ cross section at the appropriate neutron energy. This procedure is summarized in the following equations.

$$N(^{235}U(E_{ex},n,f)) = N(^{235}U(E_n + S_n(^{236}U),n,f)) \quad (12)$$

$$N(^{237}U(E_{ex},n,f)) = \frac{N(^{238}U(E_{ex},(\alpha,\alpha' f))}{N(^{236}U(E_{ex},(\alpha,\alpha' f))} \quad (13)$$

$$\times N(^{235}U(E_{ex},n,f)) \quad (14)$$

$$N(^{237}U(E_n,n,f)) = N(^{237}U(E_{ex} - S_n(^{238}U),n,f)) \quad (15)$$

The upper panel of figure 9 shows the the ^{235}U(n,f) cross section [19] used to obtain the ^{237}U(n,f) cross section. The resulting ^{237}U(n,f) cross section is plotted in the lower panel of figure 9. For completeness, the previous results from Younes and Britt [20] are also shown. The two cross sections agree well in the neutron energy range from 0 to approximately 10 MeV. Above 10 MeV our cross section is lower by approximately 10% to 20%. This difference may arise from the linear extrapolation to higher energies of first and second chance fission used by Younes and Britt.

VIII. CONCLUSIONS

The ^{237}U(n,f) cross section has been determined using the Surrogate Ratio method. This method requires that

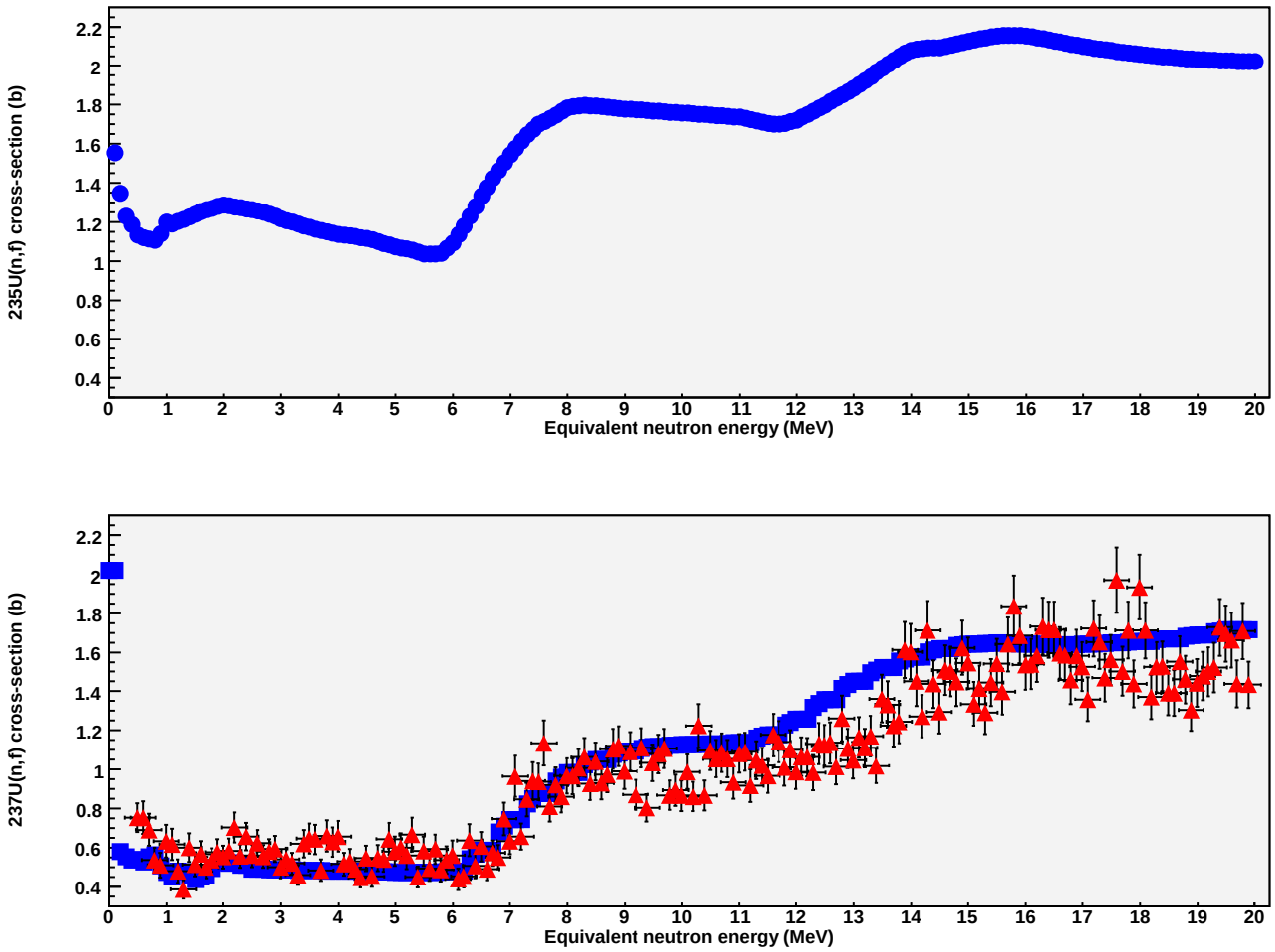

FIG. 9: The upper panel shows the ^{235}U(n,f) cross section from ENDF/B-VII [19] used to determine the ^{237}U(n,f) cross section. The lower panel compares our ^{237}U(n,f) cross section (triangles), to the results from earlier work by Younes and Britt [20] (squares, no error bars shown).

a fission cross section for a similar nucleus be known. In this experiment, the reaction $^{238}U(\alpha,\alpha' f)$ was used as a surrogate reaction for ^{237}U(n,f) and the reaction $^{236}U(\alpha,\alpha' f)$ as a surrogate reaction for the known case of ^{235}U(n,f). In using the Surrogate Ratio method, the assumption has been made that the inelastic (α,α') scattering cross section for the two nuclei (^{238}U and ^{236}U) are equal to within approximately 5%. We have also assumed that the compound nucleus formation at equivalent neutron energies in the range from 0 MeV to 20 MeV are equal to within approximately 5%. These two assumptions lead to an uncertainty in the ^{237}U(n,f) cross section no greater than 10% over the energy range from 0 to 20 MeV equivalent neutron energy. The Surrogate Ratio method minimizes uncertainties arising from pre-equilibrium decay, angular momentum effects, and fission fragment anisotropies. These adverse effects impact both reactions considered here in a similar manner and their effects are expected to approximately cancel in the Ratio method.

Acknowledgments

We wish to acknowledge the useful discussions and advice of H.C. Britt, J. Willhemy, and W. Younes. We would like to thank the 88 Inch Cyclotron operations and facilities staff for their help in performing this experiment. We also want to thank F. Howland for his effort and expertise in designing the STARS scattering chamber and R. Foreman for his efforts in manufacturing our self-supporting ^{238}U targets. This work was performed under the auspices of the U.S. Department of Energy by the University of California, Lawrence Livermore National Laboratory under contract No. W-7405-Eng-48 and Lawrence Berkeley National Laboratory under contract No. DE-AC03-76SF0098.

[1] C. Plettner *et al.*, Estimation of (n, f) cross sections by measuring reaction probability ratios. Phys. Rev. C 71, 051602(R) (2005).

[2] L.A. Bernstein *et al.*, "Surrogate Nuclear Reactions using STARS", Proceedings of the International Conference on Nuclear Data for Science and Technology (ND2004) Santa Fe, NM. AIP Conference Proceedings Vol. 769, pgs. 890-893 (2005).

[3] J. Escher and F. S. Dietrich, "Examination of the Validity of the Surrogate Ratio Method for Determining (n,f) and (n,γ) Cross Sections of Actinides," LLNL Technical Report, UCRL-TR-212509-Draft (2005) (unpublished).

[4] J. Escher and F. S. Dietrich, "Determining Cross Sections for Reactions on Unstable Nuclei: A Consideration of Indirect Approaches," Second Argonne/MSU/JINA/INT RIA Workshop: Reaction Mechanisms for Rare Isotope Beams (Michigan State University, East Lansing, March 9–12, 2005), AIP Conference Proceedings, **791** 93, (2005), UCRL-PROC-212586.

[5] J. Escher *et al.*, Nucl. Phys. A **758** (2005) 86c–89c.

[6] J. Escher *et al.*, "Surrogate Nuclear Reactions - an Indirect Method for Determining Reaction Cross Sections," Jour. Phys. G **31** S1687 (2005), UCRL-JRNL-210888.

[7] C. Forssén *et al.*, Nucl. Phys. A **758** (2005) 130c-133c.

[8] J. A. Church *et al.*, Nucl. Phys. A **758** (2005) 126c–129c.

[9] W. Younes and H. C. Britt, Phys. Rev. C **67**, 024610 (2003).

[10] W. Younes and H. C. Britt, Phys. Rev. C **68**, 034610 (2003).

[11] W. Younes, H. C. Britt, J. A. Becker, and J. B. Wilhelmy, Technical Report No. UCRL-ID-154194, Lawrence Livermore National Laboratory, Livermore, CA, 2003 (unpublished).

[12] J. D. Cramer and H. C. Britt, Phys. Rev. C **2**, 2350 (1970).

[13] J. D. Cramer and H. C. Britt, Nucl. Sci. and Eng. **41**, 177 (1970).

[14] H. C. Britt and J. B. Wilhelmy, Nucl. Sci. and Eng. **72**, 222 (1979).

[15] F. S. Dietrich, Technical Report No. UCRL-TR-201718, Lawrence Livermore National Laboratory, Livermore, CA, 2004 (unpublished).

[16] E. Gadioli and P. E. Hodgson, *Pre-Equilibrium Nuclear Reactions* (Clarendon Press, Oxford, 1992).

[17] J.T. Burke and L.W. Phair, private communication, (2005).

[18] R. Vandenbosch and J.R. Huizenga, *Nuclear Fission* (Academic Press, New York, 1973).

[19] Young, Chadwick, Talou, and Leal, ENDF/BVII β0 evaluation, MAT # 9228, Mar 2005.

[20] W. Younes and H.C. Britt, Tech. Rep. UCRL-TR-212600, Lawrence Livermore National Laboratory, (2005).